Surface Science 651 (2016) L62–L69

Contents lists available at ScienceDirect

Surface Science

journal homepage: www.elsevier.com/locate/susc

Phase diagrams for the adsorption of monomers with non-additive interactions

O.A. Pinto [a,*], A.J. Ramirez-Pastor [b], F. Nieto [b]

[a] Instituto de Bionanotecnología (INBIONATEC-CONICET), Universidad Nacional de Santiago de Estero, RN 9 Km 1125 Villa el Zanjón, Santiago del Estero G4206XCP, Argentina
[b] Departamento de Física, Universidad Nacional de San Luis, Instituto de Física Aplicada – INFAP – CONICET, Chacabuco 917, D5700BWS San Luis, Argentina

ARTICLE INFO

Article history:
Received 16 February 2016
Received in revised form 17 March 2016
Accepted 21 March 2016
Available online 24 March 2016

Keywords:
Computer simulations
Monte Carlo simulations
Equilibrium thermodynamics
Statistical mechanics

ABSTRACT

In several experimental systems phase diagrams coverage-temperature show a strong asymmetry. This behavior can be reproduced by including non-additive lateral interactions. In this work a Monte Carlo study on the canonical assembly of the criticality of monomer adsorption with non-additive interactions is presented. Traditional pairwise energies were replaced by other more general ones where the lateral interaction between two ad-atoms depends on the coverage at first sphere of coordination. This kind of energies includes multibody interactions like three-body interactions and four-body interactions, etc. These energies induce the formation of several non-additive ordered structures. Finite size scaling method was used to classify the order of phase transition of each non-additive phase. On the other hand, the corresponding phase diagrams are formed naturally, in which case the diagrams show strong asymmetries.

1. Introduction

In surface science the phase diagram of atoms or molecules is one of the most important topics for the characterization of an adsorption system. In the last few years new techniques have improved the perception of the adsorption phenomenon. Nowadays powerful experimental techniques such as LEED and STM [1] allow obtaining much information about topography of surface energy and interactions between particles deposited. Theoretically, a lattice gas model is the simplest tool for calculating phase diagrams. This method immediately induces the conservation of the vacancy-particle symmetry, which means that the diagram coverage-temperature is perfectly symmetric around half coverage when only pairwise interactions are present. However, there are several experimental systems, such as H/Pd(100) [2], H/Ru(001)[3] and Co/Cu(100), where phase diagrams are asymmetric [4]. In fact, adsorption isotherms for methane, ethane, and other adsorbates on AlPO4–5 and SAPO-5 are clearly unsymmetrical around half coverage [5–9]. The asymmetries have been theoretically studied in general in two ways: by removing the symmetry of the substrate [10] and by introducing multibody interactions like triplets (three-body interactions), and quadruplets (four-body interactions) [11,12]. Within the latter, the authors consider non-pairwise interactions, from which the idea to remove the traditional assumption of additivity arises. Non-additivity means that all lateral energies depend on the quantity of atoms in a cluster.

There are several experimental studies where additivity does not reproduce the main characteristic of the systems. For example, in Ref. [13] the line of coexistence between the condensate phase and the gas phase for Ni, Cu, Pd, and Ag on W(110) shows a strong asymmetry and a strong tendency to dimer formation. Therefore, such additivity does not satisfy these behaviors. The importance of non-additive effects has also been reported in chemisorption and catalysis [14,15]. Other examples where the additive interactions do not complete the description is in the growth of monolayer in heteroepitaxial systems with heterogeneities, such as Ag/Au(100), Ag/Pt(100), Au/Pt(100), Au/Pd(100), Au/Ag(100), Pt/Ag(100), Pt/Au(100) and Pd/Au(100) [16–18]. The formation of the electrochemistry phase in Ag on Au(111) and Au(100) [19–21] needs more complex interactions to be fully understood. Surface restructuring is another example of a system where more complex ad–ad interactions take place [22–25].

In order to explain these behaviors several models have been formulated. Some models include, for example, interactions different from pairwise interactions, or even situations where attractive and repulsive interactions compete [26]. A more complex model has been defined to describe O on W(110). This model includes interactions at nearest, next nearest, nearest-nearest neighbors, and even interactions of three and five particles to obtain an asymmetric phase diagram [27].

The non additive lateral interactions were present in [28,29] for a Grand Canonical Monte Carlo study with attractive interactions. Non-additive interactions were included in theoretical approaches for monomers and dimers [30,31]. In particular, a computational study of adsorption of repulsive monomers with non-additive interactions on square lattice were performed [32]. On the whole, the main results are: i) depending on the values of the non-additivity the c(2 × 2) ordered

* Corresponding author.
E-mail address: oapinto@unsl.edu.ar (O.A. Pinto).

http://dx.doi.org/10.1016/j.susc.2016.03.023
0039-6028/

phase (as compared to the additive case) is weakened or strengthened. It is also possible to notice the presence of different low-temperature ordered phases depending on the surface coverage. These findings are corroborated by very wide plateaus in the adsorption isotherms, steps in the isosteric heat and weak peaks in the thermodynamic factor. ii) The formation of k-mers is corroborated in a specific range of coverage and interactions. iii) There is evidence of a continuous phase transition from the c(2 × 2) structure to disorders around to half coverage for non-additive schemes. Similar results have been found in studies on the thermodynamics of adsorption on triangular and hexagonal lattices [33] and nanotube bundles [34].

For the purpose of clarity, Fig. 1 shows the snapshots of three structures formed at several surface coverages (θ), specifically at θ = 1/2, the well-known c(2 × 2), at θ = 2/3 and θ = 4/5 the dimeric and tetrameric phase respectively. The last two are new structures induced by non-additivity. This paper aims at exploring how non-additivity affects the phase diagram and the critical exponents. Consequently, Monte Carlo simulations in the canonical assembly and finite-size scaling for each phase founded in square lattices are used.

The paper is organized as follows: In Section 2, the non-additive model is presented. In Section 3, details of Monte Carlo Simulations and finite size scaling theory are given. Results and discussion of the criticality and phase diagrams are presented in Section 4. Finally, the conclusions are drawn in Section 5.

2. The theoretical model

An idealized solid surface with a square geometry of linear dimension L was considered for the analysis. A lattice-gas model with N = L × L specific adsorption sites was used. For this geometry each site has four nearest neighbors separated by a lattice constant. In order to consider the simplest possible model for non-additive ad–ad particles, a homogeneous potential surface "as seen" by an adsorbed particle shall be considered. Two kinds of energies can be taken into account, the adsorbate–substrate energy ε, and lateral interaction between i and j particles, as w_{ij}. To be more specific, a Hamiltonian can be defined as:

$$H = -\varepsilon\sum_{i=0}^{N} c_i + \sum_{i\neq j}^{N} w_{ij}c_ic_j \qquad (1)$$

where the local occupation variable c_i is 0 (1) if the adsorption site is empty (occupy). ε is independent of the temperature and coverage and can be considered equal to zero without losing generality. So as to include the non-additivity, we considered that w_{ij} depends on the occupation state of both sites i and j. The real dependence of w_{ij} on the local coverage is difficult to establish by means of an experiment. The aim of this contribution is to explore a case where the main features of the presence of non-additive interactions are kept. In order to draw general conclusions on how such interactions affect the critical behavior of thermodynamic quantities we assume that each ad-particle has four different possible configurations depending on the number of the nearest neighbors. Then, the energies are w_1, w_2, w_3 and, w_4. The lateral energy between two particles is considered to be an average of the energies of their respective environments. Fig. 2 shows an example for calculating the lateral energy between the particles 1 and 4. The multibody interactions such as triplets and quadruplet are included in the modeling as shown in Fig. 2. The real function or rule that links each energy with the number of the nearest neighbors "m" on the vicinity of adatoms is not clear. But several clues indicate that this relation could be linear. Among them, Koh and Ehrlich [35] found, by using the helium-cooled field ion microscopy technique, that the pair free energies of Pd and Ir clusters on W(110) are linear with the size. Then, it is physically reasonable to suppose that the lateral interactions depend linearly on the number of the nearest neighbors "m" on the vicinity of a given atom. So, in this model, w_m varies linearly with m and $w_z = w$, where z is the coordination number of the lattice. Following Ref. [28] we introduce the parameter of non-additivity, $P = w_1/w_z$ as a measure of the strongest to the weakest possible bonds in the system, then:

$$\frac{w_m}{w} = \frac{Pz-1}{z-1} - m\frac{P-1}{z-1}. \qquad (2)$$

This situation has been tackled by Mean Field Approach (MFA) [25] and Quasi-Chemical approach (QCA) [28,30,31]. However, the analysis given in the cited papers has been restricted to some especial cases mainly including attractive interactions. The discussion presented in the present paper covers the entire range of repulsive interactions, temperatures and coverage.

As mentioned at the beginning of this section, the present study was restricted to the case of homogeneous surfaces. More complex adsorbents (including energetic and geometric heterogeneity, surface reconstruction, anisotropy, etc.) could be treated by using a similar scheme as discussed here. Under these conditions, it is expected that the presence of a very small quantity of defects breaks down the order of the low-temperature phases. However, even though the presence of defects affects the formation of ordered structures in the adlayer, it is also expected that the phase transition survives up to a certain critical degree of disorder [36,37].

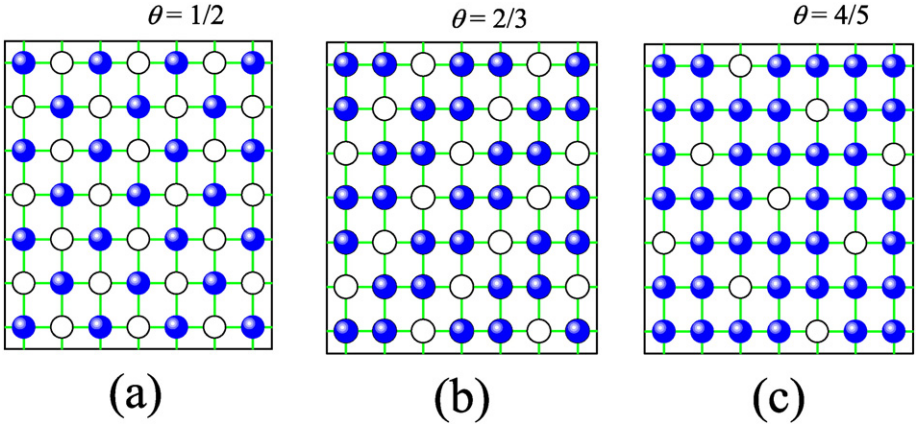

Fig. 1. Snapshot of non-additive structures. White circles correspond to empty sites and the blue ones to filled sites. A) c(2 × 2) structures, b) dimeric phase, and c) tetrameric phase. (For interpretation of the references to color in this figure legend, the reader is referred to the web version of this article.)

3. Monte Carlo simulations and finite-size scaling

Monte Carlo simulation techniques have largely been used in many areas of surface science [38–41]. One of these techniques, known as parallel tempering algorithm [42–44], was used here to study the thermodynamic properties of the Hamiltonian given by Eq. (1), from which phase diagrams can be calculated. Within the scheme of canonical assembly, the ad-atoms were placed on lattice with periodic boundary conditions. The Kawasaki dynamics [45] was applied where the Monte Carlo step was defined by L × L attempts to interchange the states of full and empty sites. The time needed for equilibration varies with the system size, temperature and coverage. Typically, the smaller system at low coverage was equilibrated with runs taking 5×10^6 MCS for each configurations, while 5×10^8 MCS were used for the larger one, with θ = 0,5 and low temperatures $T < T_c$. Large quantities of MCS were used in order to discard any metastable state. The number of MCS for averaging was always taken equal to the need for equilibration. Averages have been taken over $\approx 3 \times 10^2$ different initial configurations to calculate standard statistical error bars, and in all the plots of data and analysis shown in following sections -if error bars are not shown they are always smaller than the symbol size. Lattice sizes from L = 20 to L = 180 were simulated and the data were interpreted within the context of finite size scaling [46,47]. Most simulations were carried out on a BACO3 parallel cluster located at Instituto de Física Aplicada, Universidad Nacional de San Luís, San Luís, Argentina.

The order parameter φ adequate for describing a given phase (specific cases will be discussed in the following sections) allows to define the quantities related with its distribution such as susceptibility,

$$\chi = N^2 \frac{\left[\left\langle \varphi^2 \right\rangle_T - \langle |\varphi| \rangle_T^2\right]}{T} \tag{3}$$

and the reduced fourth-order cumulant introduced by K. Binder [48]

$$U_L(T) = 1 - \frac{\left[\left\langle (\varphi - \langle\varphi\rangle_T)^4 \right\rangle_T\right]}{3\left(\left\langle (\varphi - \langle\varphi\rangle_T)^2 \right\rangle_T\right)^2}. \tag{4}$$

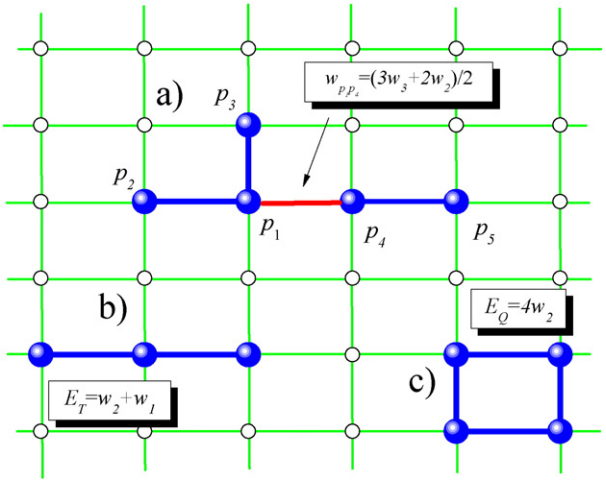

Fig. 2. a) A possible local configuration of particles and empty sites. The link energy between p_1 and p_4, represented by a red line, can be calculated as follows: the neighborhood of the p_1 is formed by three particles, p_2, p_3 and p_4, so its contribution is $3w_3$. But p_4 has only p_1 and p_5 as near neighbors, then, the link energy is $2w_2$. Finally the interaction energy between p_1 and p_4 is considered to be an average of the individual energies. b) and c) A triplet and a quadruplet with their respective energy in the non additivity scheme. In particular, if we consider additive case($P = 1.0$), the respective energies take the form of, $E_T = 2w$ and $E_Q = 4w$. (For interpretation of the references to color in this figure legend, the reader is referred to the web version of this article.)

The specific heat is sampled from energy fluctuations,

$$C_v = L^2 \frac{\left[\left\langle H^2 \right\rangle_T - \langle H \rangle_T^2\right]}{T^2} \tag{5}$$

where $<\ldots>_T$, in all the quantities, means the thermal average. The standard theory of finite size scaling [46,47] implies the following behavior of the above quantities near the critical temperature $T_C(t \equiv 1 - T/T_C)$.

$$\begin{aligned} C_v &= L^{\frac{\alpha}{\nu}} \tilde{C}\left(L^{\frac{1}{\nu}} t\right), \\ \varphi &= L^{-\frac{\beta}{\nu}} \tilde{\varphi}\left(L^{\frac{1}{\nu}} t\right), \\ \chi &= L^{\frac{\gamma}{\nu}} \tilde{\chi}\left(L^{\frac{1}{\nu}} t\right), \\ U_L &= \tilde{U}_L\left(L^{\frac{1}{\nu}} t\right), \end{aligned} \tag{6}$$

for $L \to \infty$, $t \to 0$, such that $tL^{\frac{1}{\nu}} =$ finite. Here α, β, γ and ν are standard critical exponents of the specific heat ($C_v \propto |t|^{-\alpha}$ for $L \to \infty$, $t \to 0$), order parameter ($\varphi \propto |t|^{-\beta}$ for $t > 0^+$, $L \to \infty$), susceptibility ($\chi_T \propto |t|^{\gamma}$for $L \to \infty$, $t \to 0$) and correlation length ξ ($\xi \propto |t|^{-\nu}$ for $L \to \infty$, $t \to 0$), respectively. $\tilde{C}, \tilde{\varphi}, \tilde{\chi}$ and $\tilde{U}_L$ are scaling functions for the respective quantities. As it is well known, Eq. (6) provide various efficient routes to extract estimates for both T_c and the critical exponents from Monte Carlo data, and these methods must be discussed in the context of our model.

One can calculate the critical temperature of the phase transition from the intersection of cumulants and from the extrapolation of the positions $T_c(L)$ of the maxima of the slopes of φ, $(d\varphi/dT)_{\max}$ and $U_L(T)$, $(dU_L/dT)_{\max}$, as well as of the susceptibility maxima, $\chi_T^{\max}$, respectively. For these quantities one expects, from Eq. (6), that

$$T_C(L) = T_C(\infty) + \text{const}\, L^{-\frac{1}{\nu}}, \quad L \to \infty \tag{7}$$

where $T_C(\infty)$is the critical temperature of the infinite system and the constant depends on the considered quantity. From cumulants intersection, one can also deduce $T_C(\infty)$and using υ as an effective exponent deduced from a fit of $[(dU_L/dT)_{\max}]$ to a power law,

$$\left(dU_L \Big/ dK\right)_{\max} \propto L^{1/\nu}. \tag{8}$$

From Eqs. (6) to (8) it is possible to estimate *Tc* and $1/\nu$, therefore it is expected to scale the full data for $\tilde{C}, \tilde{\varphi}, \tilde{\chi}$ and $\tilde{U}_L$ in "data collapsing" plots. Note that the analysis given above is valid only for sufficiently large *L* and for *t* in the asymptotic critical regime. However, this analysis can be applied to the entire range of *L* and *T* if the data fall in the "domain of attraction" of a simple fixed point characterizing only one universality class of critical phenomena.

4. Phase diagram at finite temperature

In the last section the methodology used to obtain the critical temperature as a function of the coverage for different cases was discussed. In the following section, the behavior of the thermodynamic quantities in different regions of the phase diagram is analyzed. Finally, the complete phase diagram for finite temperature is presented and discussed.

4.1. The c(2 × 2) phase

In order to describe the system in the region of low-temperature ordered phase c(2 × 2), it is convenient to define the following geometrical order parameter:

$$\varphi_{c(2x2)} \equiv \frac{|\theta_1 - \theta_2|}{2} \tag{9}$$

where θ_1 and θ_2 are average coverages for the two sub-lattices trivially defined by the c(2 × 2) phase. So as to illustrate how the Monte Carlo scheme was used to obtain the phase diagram we present the scaling analysis for $\theta = 0{,}5$ and $P = 0{,}7$. Fig. 3a, b and c shows the behavior of the order parameter, the susceptibility and the specific heat as a function of the temperature at several values of the size system. In the three variables a typical behavior of the phase transition can be observed. There are finite size effects as L tends to be infinite. An order–disorder phase transition occurs in the additive situation, and the critical exponents correspond to Ising lattice-model in two dimensions (Potts model with q = 2). From the intersections of U_L, we can get the estimation of the critical temperature, $k_BT_C(P = 0.7) = 0.433(2)$. With these data we can apply the Eq. (6) and get the collapses of the curves as it is shown in Fig. 3d, e and f, we use $\nu = 1.0$, $\beta = 1/8$, $\alpha = 0.0(\log)$ and $\gamma = 7/4$. Now, the behavior of fourth-order cumulants is described. Fig. 4a shows the cumulant of the order parameter for different size L. The intersections at the critical temperature can be observed, and $U_L^* = 0.619(2)$ in complete accordance with the Ising model [49] were found. Fig. 4b shows the collapses. Other interesting quantity is the fourth-order cumulant of energy. Using the same definition in Eq. (4), where we replace the order parameter and its moments by the energy per site and its moments, we obtain:

$$U_{LE}(T) = 1 - \frac{\left[\left\langle E^4 \right\rangle_T\right]}{3\left(\left\langle E^2 \right\rangle_T\right)^2}, \tag{10}$$

this parameter is useful to define the kind of phase transition. U_{LE} has a minimum close to the critical point, as the size of systems tends to the thermodynamics limit($L \to \infty$), this minimum tends to 2/3, in complete concordance with the Ising lattice-model as it is plotted in Fig. 4c. As we know from [32,33] at this coverage, the non- additivity only reinforces the c(2 × 2) phase as P changes. We have verified that for all values of P where the c(2 × 2) phase is formed, the critical behavior is similar to the additive case.

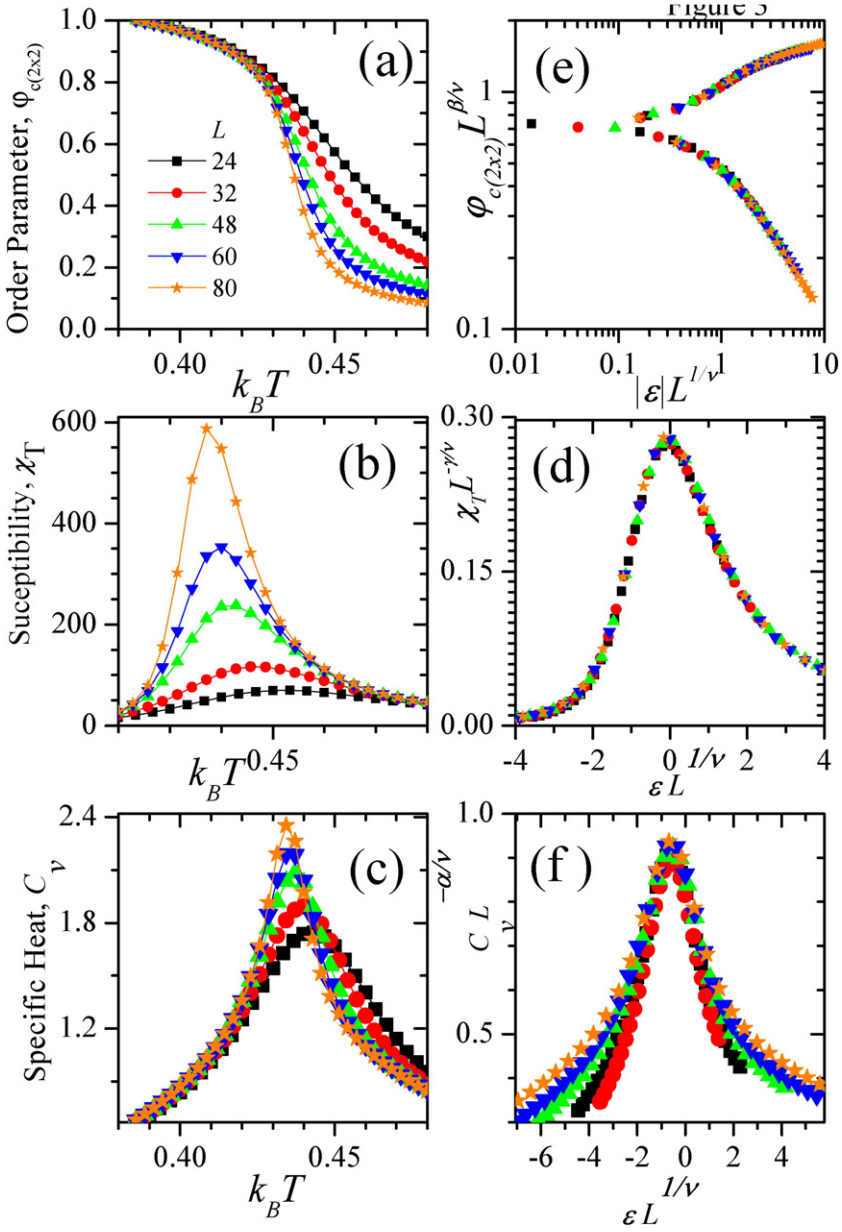

Fig. 3. Several thermodynamics parameter versus kT, for c(2 × 2) ordered phase as a function of the size L for $P = 0.7$ and $\theta = 1/2$. a) Order parameter, b) susceptibility, and c) specific heat. The corresponding collapses of the curves are shown in d), e) and f).

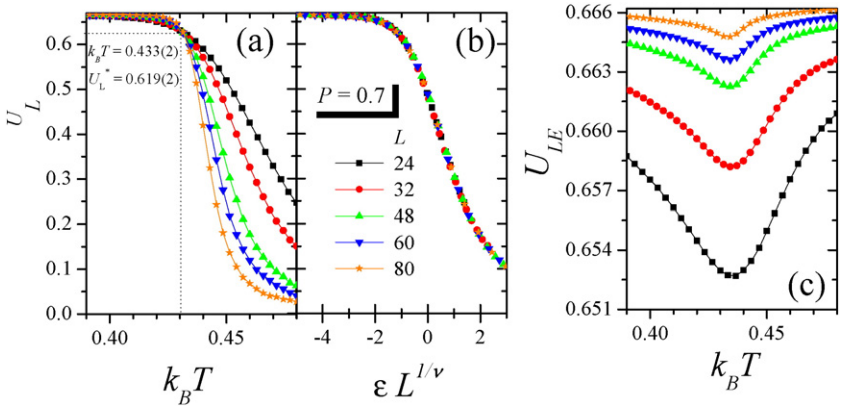

Fig. 4. For c(2 × 2) ordered phase at θ = 1/2. a) Fourth-order cumulant of the order parameter for different size *L*. b) Curve collapses. c) Fourth-order cumulant of energy.

4.2. The dimeric phase

The dimeric phase is characterized by domains of parallel "zig-zag" strips oriented at $\pm 45^{\circ}$ from the lattice symmetry axes, separated from each other by strips of single empty sites (Fig. 1b). This phase is formed at $\theta = 2/3$ for $P < 0.4$. There are six different configurations with the same energy, and each one situated in a sub-lattice. In order to describe it, we define an order parameter as:

$$\varphi_z \equiv b \sum_{i,j} |\delta_i - \delta_j| \tag{11}$$

here δ_i and δ_j are the density of empty sites for the "*i*" and "*j*" sub-lattices respectively. The summation of the differences are taken over the six sub-lattices, *b* is normalization constant. For $T < Tc$ one configuration is formed in all lattice then $\varphi_z = 1.0$ but $T > Tc$ the systems is completely disordered and $\varphi_z \approx 0.0$. For the analysis we set the system at $P = 0.3$ and $\theta = 2/3$. Fig. 5a and b show the cumulant of the order parameter and the energy for several values of *L*. In both cases the behavior is similar to an order–disorder phase transition. The U_L is always positive. The energy cumulant presents a minimum whose values tend to 2/3, as *L* tends to infinite, in a similar form to c(2 × 2) phase. There is strong evidence that the dimeric phase corresponds to an order–disorder phase transition. On the other hand, the cumulant of order parameter presents an intersection where the critical temperature can be established; in this case, we have $k_BTc(P = 0.3, \theta = 2/3) = 0.22(1)$ and $U_L = 0.64(2)$. At this point the critical exponents can be estimated by the fluctuation methods [49–53]. The ν exponent can be obtained from different variables, for example, by the maxima of the derivative of U_L or the logarithmic derivatives of $\langle\varphi_z\rangle$ and $\langle\varphi^2{}_z\rangle$ in all cases from inverse of temperature *K*. More explicitly, ν can be obtained as:

$$\left.\frac{d\log\langle F\rangle}{dK}\right|_{\max} \sim L^{\frac{1}{\nu}} \tag{12}$$

where *F* can be U_L, $\langle\varphi_z\rangle$ or $\langle\varphi^2{}_z\rangle$. On the other hand, α/ν and γ/ν can be obtained by the maximums of $C_v$and χ respectively. Following these ideas, the relation can be obtained at the point of inflection of the order parameter i.e. where $d\langle\varphi_z\rangle/dK$ is maximal, so:

$$\left.\frac{d\log\langle\varphi_z\rangle}{dK}\right|_{\max} \sim L^{\left(\frac{1-\beta}{\nu}\right)}. \tag{13}$$

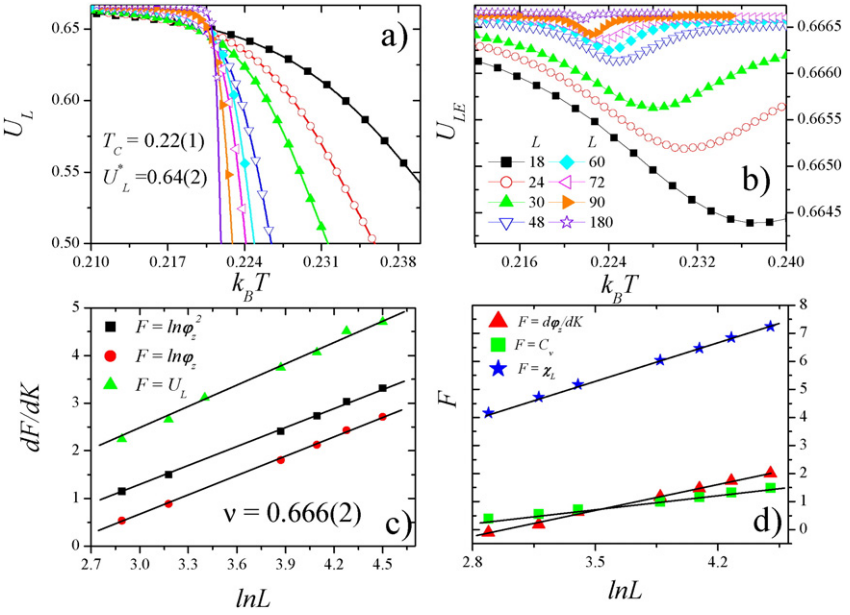

Fig. 5. For the dimeric phase at $P = 0.3$ and θ = 2/3. a) Fourth-order cumulant of energy. b) Fourth-order cumulant of the order parameter. c) The derivative of *F* versus ln*L*, and the linear fits. c) *F* versus ln*L*.

Fig. 5c shows the derivative of F versus ln$L$, and by means of linear fits of the three variables the same value of $\nu = 0.666(2)$ is obtained. The other relations between exponents are plotted in Fig. 5d; we found $((1-\beta)/\nu) = 1.353(3))$, $\alpha/\beta = 0.788(5)$ and $\gamma/\nu = 1.914(5)$ With these relations, the Rushbrooke [54] equality can be applied, which relates the critical exponents as:

$$\frac{\alpha}{\nu} + \frac{2\beta}{\nu} + \frac{\gamma}{\nu} = \frac{2}{\nu}. \tag{14}$$

The exponents measured satisfy the last relation. With these exponents the scaling relations for the collapses of the thermodynamics values can be applied, as shown in Fig. 6(a–d). The values of these critical exponents within the statistical errors are close to the universality of Potts model with q = 4 [55,56].

The q-state Potts model [55,56] consists of a lattice of spins, which can take q different values. For q = 2 [c(2 × 2) phase], the Potts model is equivalent to the Ising model. In the case of q = 4 (dimeric phase), the model corresponds to the well-known Ashkin–Teller model [55,57]. In general, the Potts model is likely to have extensive applications in lattice statistics and critical phenomena. Interested readers are referred to Ref. [55] for a more complete description of the Potts model and its implications and applications.

4.3. The tetrameric phase

For the critical analysis of the tetrameric phase we need to define an order parameter φ_t, like the Eq. (11). The only difference is that this phase has eight different configurations for the same energy. The quantities φ_t, C_v, U_{LE} and U_L were calculated for $P = 0.2$ and $\theta = 4/5$ at different values of L. In Fig. 7a we observe how the φ_t tends to a step as L tends to infinite. The C_v and C_L have a typical behavior of a phase transition as it is shown in Fig. 7b and c respectively. In all cases there are typical effect sizes. C_L has a negative minimum that is more intense as L increases. It is important to observe that φ_t do not cross each other. U_{LE} has an intense minimum that does not disappear for large L as it is shown in Fig. 7d. However, we calculate the distribution for φ_t and energy per site (not shown here by simplicity) and both have two well-defined maximums in complete concordance with a first order phase transition as it is described in [58]. As it is known, quantities at a first order phase transition scale to the volume of the systems as $T_C(\infty) + const L^{-d}$. The inset in Fig. 7d shows the dependence of $T_C(L)$ versus L^{-2}, and it is possible to obtain $Tc(P = 0.3) = 0.1188(6)$ by means of a linear fit.

4.4. The phase diagram

Following with the study, now we are in condition to plot the phase diagram T-θ for the non-additive interactions. As we have said before we have two methods to obtain the critical temperature, i) the intersection of cumulants, and ii) any manifestations of the physics quantities obtained with the Eq. (7). For the order–disorder phase transition both methods are applicable, but for first order phase transition only the second is useful. For the c(2 × 2) and dimeric phase the intersection of U_L at different values of (θ, P) was used. The phase diagram is shown in Fig. 8.The critical temperatures are normalized at the additive case, $T_C(P = 1.0, \theta = 1/2) = 0.567$. P is varied from 0.2 to 1.4. We begin the description by the c(2 × 2) structure. For $T < T_C$ the c(2 × 2) structure is formed as it is expected. The additive curve $P = 1.0$ is symmetric around half coverage (green triangle in Fig. 8) because the vacancy-particle symmetry is satisfied. As $P < 1.0$ we can observe a non-additivity effect, the curves begin to be asymmetric and smaller than in the additive case. This means than c(2 × 2) structure is weaker, in complete concordance with the previous thermodynamics analysis [32].This asymmetry is more evident as P tends to zero -for clarity the first dash line indicates the half coverage. For $P > 1.0$ the situation is the opposite, the curves are bigger and more asymmetric than in the additive case. The dependence of the temperature on P is in perfect concordance with the analysis done in [59], where a linear dependence on P, for c(2 × 2), is established.

The dimeric and tetrameric phase are completely formed at $\theta = 2/3$ and 4/5, respectively for $P < 0.4$. The respective diagrams are shown in

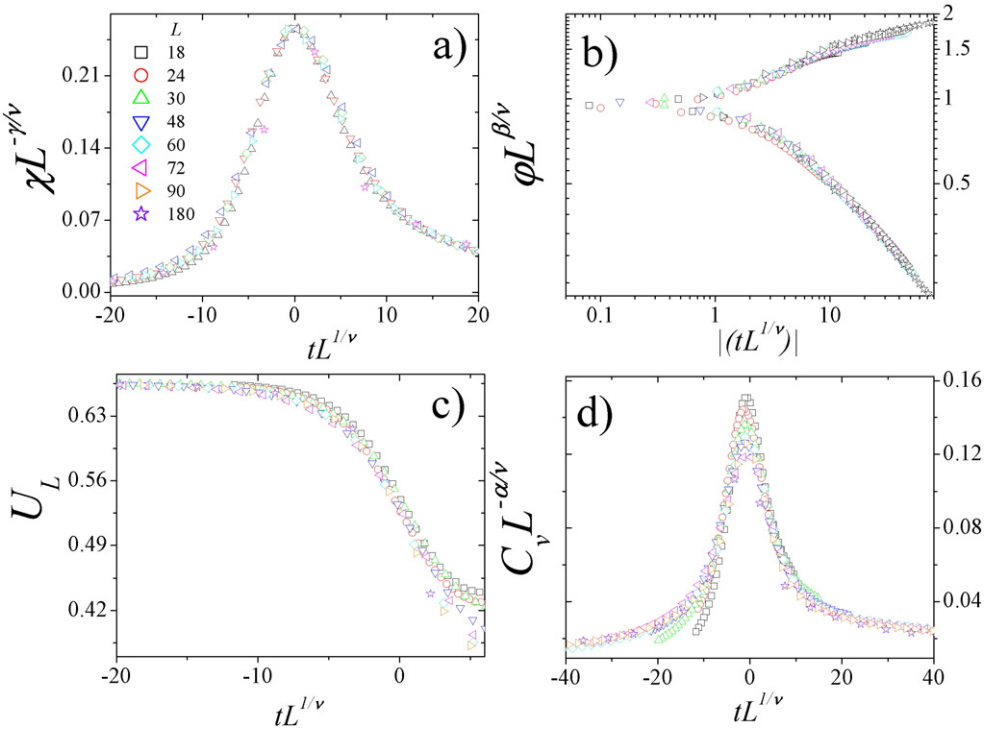

Fig. 6. Collapses of the thermodynamics parameters for the dimeric phase at $P = 0.3$ and $\theta = 2/3$. a) Susceptibility, b) Order parameter, c) Fourth-order cumulant of the order parameter and d) Specific heat.

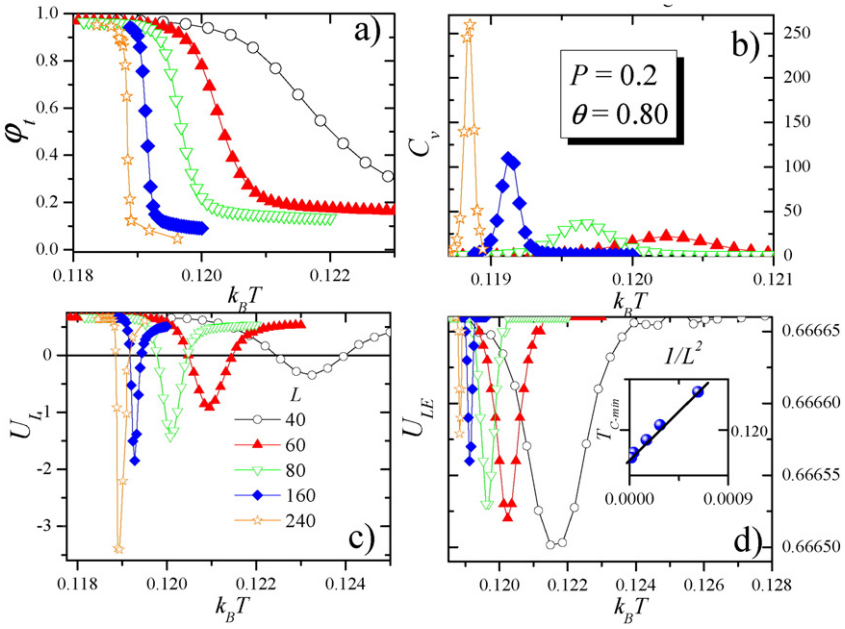

Fig. 7. For the tetrameric phase at $P = 0.2$ and $\theta = 4/5$. a) Order parameter, b) Specific heat, c) Fourth-order cumulant of the order parameter, and d) Fourth-order cumulant of the energy.

Fig. 8. For these cases the biggest curve corresponds to $P = 0.2$, contrary to what happens to c(2 × 2) structure. In all cases the diagrams are asymmetric. As expressed before, the second- and third-dash line denote, $\theta = 2/3$ and 4/5. To quantify the asymmetric character of the diagrams, it is convenient to define a symmetry parameter S. This parameter quantifies the asymmetry. In typical diagrams it is possible to define a reference coverage θ_R, and it corresponds to the coverage where the structure occupies all the substrate without imperfections. Then S can be defined as:

$$S(P) = \frac{\int_0^{\theta_R} T_C(\theta, P)d\theta}{\int_{\theta_R}^{1} T_C(\theta, P)d\theta}, \tag{15}$$

where the integral in the numerator[denominator] is the area on the left[right] of θ_R in the phase diagram. The reference coverages are: 1/2, 2/3 and 4/5 corresponding to c(2 × 2), dimeric and tetrameric phase respectively. When the diagram is symmetric S is one. We can define two regimens for the asymmetries: Asymmetry of type I [II] when $S < 1.0$[$S > 1.0$] indicates that the diagram is asymmetric because the left area > right area [right area > left area]. Fig. 9 presents S versus P for all the phases studied. The dash lines indicate the intersection of $P = 1.0$ and $S = 1.0$, and correspond to the additive scheme and the symmetric diagram. For the c(2 × 2) phase diagram at values $P < 1.0$ the asymmetry is type I and $P > 1.0$ is type II. For the other structures we can observe that in all cases the curves are type I.

5. Conclusions

In this work the critical behavior of non-additive lateral interactions associated to adsorption phenomenon is analyzed. The traditional assumption of additive interaction is reformulated to include many body interactions in the non-additive language. We consider that the lateral interaction depends on the occupation in its neighborhood. The study was done within the scheme of lattice-gas model with square geometry. In previous works the formations of new structures like the dimeric and the tetrameric phase were found in thermodynamics studies. We can draw several important conclusions from this work.

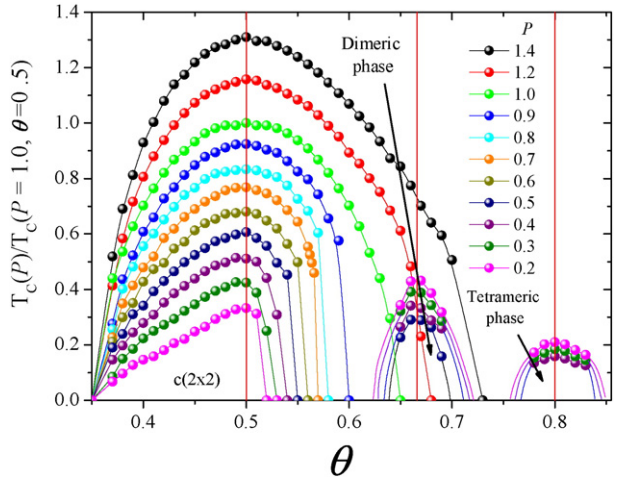

Fig. 8. Phase diagram ,θ-T for the three non-additive phases. Dash lines indicate the coverages 1/2, 2/3 and 4/5.

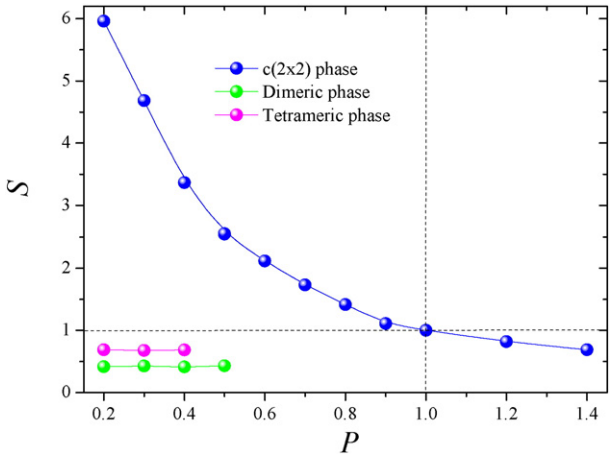

Fig. 9. Asymmetry parameter S versus P. The intersection of the dash lines indicates the symmetric conditions.

1. The c(2 × 2) ordered structure formed with non-additive interactions are in complete concordance with the order–disorder phase transition with the Ising 2D (Potts model with q = 2) critical exponents. The collapses of curves corroborate this conclusion.
2. The dimeric phase is characterized by order–disorder phase transitions with critical exponents that correspond, with the statistical errors, with the universality of Potts model with q = 4.
3. The critical behavior for tetrameric phase corresponds to a first order phase transition.
4. The θ-T phase diagram has been calculated for different condition of non-additivity.

We observe how a strong asymmetry is induced by this kind of interactions. The asymmetries for c(2 × 2) is stronger as the non-additivity parameter is different from one. For the dimeric and tetrameric phase, the structures are asymmetric in all cases.

This kind of interactions can be responsible for the strong asymmetries observed in experimental studies.

Acknowledgments

O.A.P. acknowledges financial support from Universidad Nacional de Santiago del Estero, Argentina, under project CICyT UNSE 23A173.

References

[1] D.P. Woodruff, T.A. Delchar, Modern Techniques of Surface Science, Cambridge University Press, 1994.
[2] R.J. Behm, K. Christmann, G. Ertl, Surf. Sci. 99 (1980) 320.
[3] P. Uvdal, P.-A. Karlsson, C. Nyberg, S. Andersson, N. Richardson, Surf. Sci. 202 (1988) 167.
[4] M. Sokolowski, T. Koch, H. Pfnür, Surf. Sci. 243 (1991) 261.
[5] A. Boutin, R.J.-M. Pellenq, D. Nicholson, Chem. Phys. Lett. 219 (1994) 484.
[5] V. Lachet, A. Boutin, R.J.-M. Pellenq, D. Nicholson, A.H. Fuchs, J. Phys. Chem. 100 (1996) 9006.
[7] R. Radhakrishnan, K. Gubbins, Phys. Rev. Lett. 79 (1997) 2847.
[8] T. Maris, T.J.H. Vlugt, B. Smit, J. Phys. Chem. 102 (1998) 7183.
[9] C. Martin, N. Tosi-Pellenq, J. Patarin, J.P. Coulomb, Langmuir 14 (1998) 1774.
[10] B.N.J. Persson Surface, Science 258 (1991) 451.
[11] T.L. Einstein, R. Sathiyanarayanan, in: M. Michailov (Ed.), Nanophenomena at surfaces: fundamentals of exotic condensed matter properties, Springer Berlin Heidelberg 2011, p. 19.
[12] M. Sandhoff, H. Pfnür, H.-U. Everts, Surf. Sci. 280 (1993) 185.
[13] J. Kolaczkiewicz, E. Bauer, Surf. Sci. 151 (1985) 333.
[14] M.E. Ruíz, J. Garcia-Prieto, W.L. Feng, O. Novaro, J. Mol. Catal. 33 (1985) 311.
[15] M.E. Ruíz, O. Novaro, J. Garcia-Prieto, J. Mol. Catal. 40 (1987) 37.
[16] M.C. Giménez, E.P.M. Leiva, Langmuir 19 (2003) 10538.
[17] M.I. Rojas, M.C. Giménez, E.P.M. Leiva, Surf. Sci. Lett. 581 (2005) L109.
[18] M. Cecilia Giménez, E.V. Albano, J. Phys. Chem. C 111 (2007) 1809.
[19] M.C. Giménez, M.G. del Popolo, E.P.M. Leiva, Electrochem. Acta 45 (1999) 699.
[20] M.C. Giménez, M.G. del Popolo, E.P.M. Leiva, S.G. Garca, D.R. Salinas, C.E. Mayer, W.J. Lorenz, J. Electrochem. Soc. 149 (2002), E109.
[21] M.C. Giménez, M.G. del Popolo, E.P.M. Leiva, Langmuir 18 (2002) 9087.
[22] W.H. Ching, D. Huber, M.G. Lagally, G.-C. Wang, Surf. Sci. 77 (1979) L497.
[23] K. Binder, D.P. Landau, Surf. Sci. 108 (1981) 503.
[24] L.C.A. Stoop, Thin Solid Films 103 (1983) 375.
[25] K. Kaski, W. Kinzel, J.D. Gunton, Phys. Rev. B 27 (1983) 6777.
[26] W. Selke, K. Binder, W. Kinzel, Surf. Sci. 125 (1983) 74.
[27] P.A. Rikvol, K. Kaski, J.D. Gunton, M.C. Yalabik, Phys. Rev. B 29 (1984) 11.
[28] A. Milchev, K. Binder, Surf. Sci. 164 (1985) 1.
[29] A. Milchev, J. Chem. Phys. 78 (1983) 1994.
[30] A. Milchev, M. Paunov, Surf. Sci. 108 (1981) 25.
[31] A. Milchev, Electrochem. Acta 28 (1983) 941.
[32] O.A. Pinto, A.J. Ramirez-Pastor, F. Nieto, Surf. Sci. 602 (2008) 1763.
[33] O.A. Pinto, A.J. Ramirez-Pastor, F. Nieto, Phys. A 389 (2010) 3456.
[34] O.A. Pinto, P.M. Pasinetti, A.J. Ramirez-Pastor, F. Nieto, J. Chem. Phys 134 (2011) (064702).
[35] S.J. Koh, G. Ehrlich, Phys. Rev. B 60 (1999) 8.
[36] G. Chmiel, A. Patrykiejew, W. Rzysko, S. Sokolowski, Phys. Rev. B 48 (1993) 14454.
[37] M.A. Perarnau, P.M. Centres, F. Bulnes, A.J. Ramirez-Pastor, Phys. Chem. Chem. Phys. 12 (2010) 13280.
[38] A. Patrykiejew, S. Sokolowski, K. Binder, Surf. Sci. Rep. 37 (2000) 207.
[39] K.A. Fichthorn, W.H. Weinberg, J. Chem. Phys. 95 (1991) 1090.
[40] K.A. Fichthorn, M.L. Merrick, M. Scheffler, Appl. Phys. A Mater. Sci. Process. 75 (2002) 17.
[41] K.A. Fichthorn, Y. Lin, J. Chem. Phys. 138 (2013) 164104.
[42] K. Hukushima, K. Nemoto, J. Phys. Soc. Jpn. 65 (1996) 1604.
[43] P.M. Pasinetti, F. Romá, A.J. Ramirez-Pastor, J. Phys. Chem. C 136 (2012) (064113).
[44] N. Metropolis, A.W. Rosenbluth, M.N. Rosenbluth, A.H. Teller, E. Teller, J. Chem. Phys. 21 (1953) 1087.
[45] K. Kawasaki, Phys. Rev. 145 (1966) 224.
[46] D.J. Earl, M.W. Deem, Phys. Chem. Chem. Phys. 7 (2005) 3910.
[47] P.M. Pasinetti, F. Romá, J.L. Riccardo, A.J. Ramirez-Pastor, Phys. Rev. B 74 (2006) 155418.
[48] K. Binder, Z. Phys. B 43 (1981) 119.
[49] K. Binder, D.P. Landau, Surf. Sci. 151 (1985) 409.
[50] A.M. Ferrenberg, D.P. Landau, Phys. Rev. B 44 (1991) 5081.
[51] W. Janke, M. Katoot, R. Villanova, Phys. Rev. B 49 (1994) 9644.
[52] K. Binder, E. Luijten, Phys. Rep. 344 (2001) 179.
[53] F. Romá, J.L. Riccardo, A.J. Ramirez-Pastor, Phys. Rev. B 77 (2008) 195401.
[54] G.S. Rushbrooke, J. Chem. Phys. 39 (1963) 842.
[55] F.Y. Wu, Rev. Mod. Phys. 54 (1982) 1.
[56] R.B. Potts, Proc. Camb. Phil. Soc. 48 (1952) 106.
[57] J. Ashkin, E. Teller, Phys. Rev. 64 (1943) 178.
[58] M.S.S. Challa, D.P. Landau, K. Binder, Phys. Rev. B 34 (1986) 1841.
[59] O.A. Pinto, A.J. Ramirez-Pastor, F. Nieto, Phys. A 391 (2012) 6390.